

Temperature controlled Fe/Au/FeRh spin valves

P. Drózdź, M. Ślęzak, K. Matlak, A. Koziół-Rachwał, D. Wilgocka-Ślęzak, J. Korecki, and T. Ślęzak

Citation: *AIP Advances* **8**, 101434 (2018); doi: 10.1063/1.5042841

View online: <https://doi.org/10.1063/1.5042841>

View Table of Contents: <http://aip.scitation.org/toc/adv/8/10>

Published by the [American Institute of Physics](#)

Articles you may be interested in

[Effect of strain and thickness on the transition temperature of epitaxial FeRh thin-films](#)

Applied Physics Letters **111**, 172401 (2017); 10.1063/1.4997901

[Effect of epitaxial strain and lattice mismatch on magnetic and transport behaviors in metamagnetic FeRh thin films](#)

AIP Advances **7**, 056314 (2017); 10.1063/1.4976301

[Strain effects on the magnetic order of epitaxial FeRh thin films](#)

Journal of Applied Physics **124**, 085306 (2018); 10.1063/1.5020160

[Reversible and magnetically unassisted voltage-driven switching of magnetization in FeRh/PMN-PT](#)

Applied Physics Letters **113**, 152901 (2018); 10.1063/1.5040184

[Epitaxial strain controlled magnetocrystalline anisotropy in ultrathin FeRh/MgO bilayers](#)

AIP Advances **7**, 055914 (2017); 10.1063/1.4974059

[Structural, magnetic, and transport properties of Fe_{1-x}Rh_x/MgO\(001\) films grown by molecular-beam epitaxy](#)

Applied Physics Letters **113**, 082403 (2018); 10.1063/1.5048303



Don't let your writing
keep you from getting
published!

AIP | Author Services

Learn more today!

Temperature controlled Fe/Au/FeRh spin valves

P. Drózdź,^{1,a} M. Ślęzak,¹ K. Matlak,¹ A. Kozioł-Rachwał,¹
D. Wilgocka-Ślęzak,² J. Korecki,^{1,2} and T. Ślęzak¹

¹AGH University of Science and Technology, Faculty of Physics and Applied Computer Science,
Aleja Adama Mickiewicza 30, 30-059 Kraków, Poland

²Jerzy Haber Institute of Catalysis and Surface Chemistry, Polish Academy of Sciences,
30-239 Kraków, Poland

(Received 5 June 2018; accepted 12 October 2018; published online 30 October 2018)

We demonstrate that FeRh layers can be implemented to the epitaxial Fe/Au/FeRh spin valve structures grown on MgO(001). Owing to the AFM-FM phase transition in the FeRh film, the magnetic structure of our Fe/Au/FeRh system can be temperature controlled. The indirect exchange coupling between Fe and FeRh films mediated by the Au spacer enables to control the relative orientation of the Fe and FeRh magnetizations by the Au spacer thickness between ferromagnetic and non-collinear with nearly orthogonal magnetizations. Moreover, the evolution of magnetic structure of the Fe/Au/FeRh system along with the AFM-FM transition is accompanied by the reversible in-plane rotation of the top Fe-layer magnetization. © 2018 Author(s). All article content, except where otherwise noted, is licensed under a Creative Commons Attribution (CC BY) license (<http://creativecommons.org/licenses/by/4.0/>). <https://doi.org/10.1063/1.5042841>

The FeRh alloy with equiatomic composition reveals a temperature induced first-order magnetic transition from antiferromagnetic (AFM) to ferromagnetic (FM) state at a transition temperature close to 350-K.¹⁻³ This unique AFM-FM transition is accompanied by a volume expansion,^{4,5} a decrease of resistivity,¹ and a large change in entropy.^{6,7} Recently, low dimensional FeRh films exhibiting AFM-FM transition have attracted a lot of attention, as they are promising materials for new storage media applications, such as heat assisted magnetic recording (HAMR).^{8,9} In our previous paper we showed that AFM-FM phase transition in FeRh system can be utilized to reversibly switch magnetization of a cobalt ultrathin film that is directly exchange coupled to the epitaxial FeRh layer.¹⁰ In this report we demonstrate how the FeRh layers can be implemented to the epitaxial Fe/Au/FeRh spin valve structures grown on MgO(001). Owing to the AFM-FM phase transition in FeRh film, the magnetic structure of our Fe/Au/FeRh system can be temperature controlled between Fe/Au/FeRh_{FM} and Fe/Au/FeRh_{AFM} states, where FeRh_{FM} and FeRh_{AFM} refer to the ferromagnetic and antiferromagnetic state of the FeRh sublayer, respectively. The indirect exchange coupling between Fe and FeRh films mediated by the Au spacer enables control of the relative magnetization orientation of Fe and FeRh magnetizations in Fe/Au/FeRh_{FM} by the Au spacer thickness between collinear (ferromagnetic) and non-collinear with nearly orthogonal magnetization orientation. Moreover, the evolution of the Fe/Au/FeRh magnetic structure along with the AFM-FM transition is accompanied by the reversible, in-plane rotation of the top Fe layer magnetization.

The equiatomic FeRh layer with a thickness of 200-Å was grown by molecular beam epitaxy (MBE) via co-deposition on the MgO(001) substrate at 670-K followed by annealing at 1300-K for 30-min to promote formation of the desired B2 structure. Next, epitaxial Au wedge-shaped film with thickness varying from 4-Å to 40-Å was deposited at room temperature. Finally, the Fe layer with a thickness of 50-Å was evaporated on the Au(001) surface. Growth of the Au spacer and the top Fe layer was followed by a 15-min annealing of the whole system at 500 K. The structure of the films was monitored at each preparation step by low energy electron diffraction (LEED). The FeRh pattern

^apiotr.drozd@fis.agh.edu.pl



is characterized by sharp diffraction spots and low background indicating a high structural quality of the FeRh system. Comparison of the LEED patterns (not shown) of the MgO substrate and FeRh alloy indicates a 45° in-plane rotation of the MgO and B2 FeRh lattices. Similar rotational relations were found between the FCC Au(001) and the FeRh surface, as well between the Fe(001) film and the Au(001) surface.

The magnetic properties were studied in-situ with longitudinal magneto-optical Kerr effect (LMOKE). The LMOKE characterization was performed in the two separate measurement sequences. First the AFM-FM phase transition of Au/FeRh/MgO system was studied. To obtain the temperature dependence of the FeRh magnetization, the LMOKE magnetic hysteresis loops were collected in a wide temperature range and the value of Kerr rotation at saturation (ROT_{SAT}) (normalized to the ROT_{SAT} at 452-K) was taken as a measure of the FeRh magnetization in a similar way as in Ref. 10. Exemplary hysteresis loops (normalized in the same procedure) collected with the external magnetic field applied along the [100] in-plane direction and the temperature dependence of normalized Kerr rotation at saturation ($ROT_{SAT}(T)$) obtained for the FeRh sublayer are shown in Fig. 1a and Fig. 1b, respectively. Blue and red arrows indicate branches collected during the cooling and heating, respectively. It is clear from the Fig. 1b that the FeRh alloy film has revealed a temperature induced first-order magnetic transition from an antiferromagnetic (AFM) to ferromagnetic (FM) state. The temperature profile of the transition (that is independent on the Au thickness as checked by LMOKE) is characterized by a thermal hysteresis with the width of about 30 K and a clear shift to higher temperatures as compared to the bulk.¹ The increase of the transition temperature could be induced by a surface strain exerted on the FeRh by the Au spacer, but effects of Au interdiffusion to the FeRh layer cannot be excluded.¹¹ It seems, that within the LMOKE sensitivity (that is in a monolayer range) the ferromagnetic phase disappears completely at the FM-AFM transition in contrast to the recent literature data showing for uncoated FeRh films a stable ferromagnetic phase near the film surface that is not participating in the AFM-FM transition.¹²

The second series of the LMOKE measurements corresponds to the Fe/Au/FeRh system. A sketch of the sample is presented in Fig. 2a. The magnetic hysteresis loops were measured as a function of Au spacer thickness, d_{Au} , in the temperature range matching the temperature profile of the AFM-FM phase transition in the FeRh film that was shown in Fig. 1b. The external magnetic field could be applied along both [100] and [010] in-plane MgO directions. The hysteresis curves collected with external magnetic field along [100] for the selected Au spacer thicknesses, $d_{Au}=15\text{-}\text{\AA}$ and $24\text{-}\text{\AA}$, at temperatures corresponding to the $FeRh_{AFM}$ state (blue loops collected at 310 K) and $FeRh_{FM}$ state (red loops collected at 440-K) are shown in Fig. 2b. The LMOKE loops acquired at 310-K were always rectangular, independently on the Au spacer thickness (see blue loops in Fig. 2b) indicating [100] easy magnetization direction of Fe film. However, at the temperature corresponding to the FM state of the FeRh alloy, the relative orientation of the Fe and FeRh magnetization changes with increasing Au spacer thickness between collinear (ferromagnetic) and non-collinear (see red loops in Fig. 2b). The shape of the loop acquired for the $24\text{-}\text{\AA}$ Au spacer, characterized by the higher

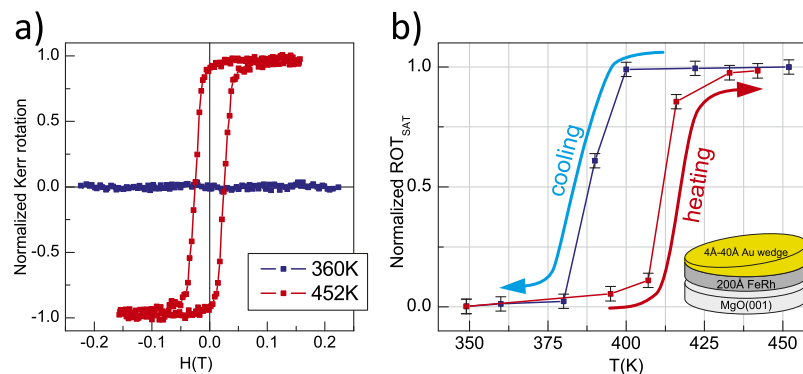


FIG. 1. a) Exemplary LMOKE magnetic hysteresis loops acquired for AFM (360-K) and FM (452-K) state of the FeRh alloy covered by Au wedge. b) The temperature profile of the AFM-FM transition for Au/FeRh (200-Å).

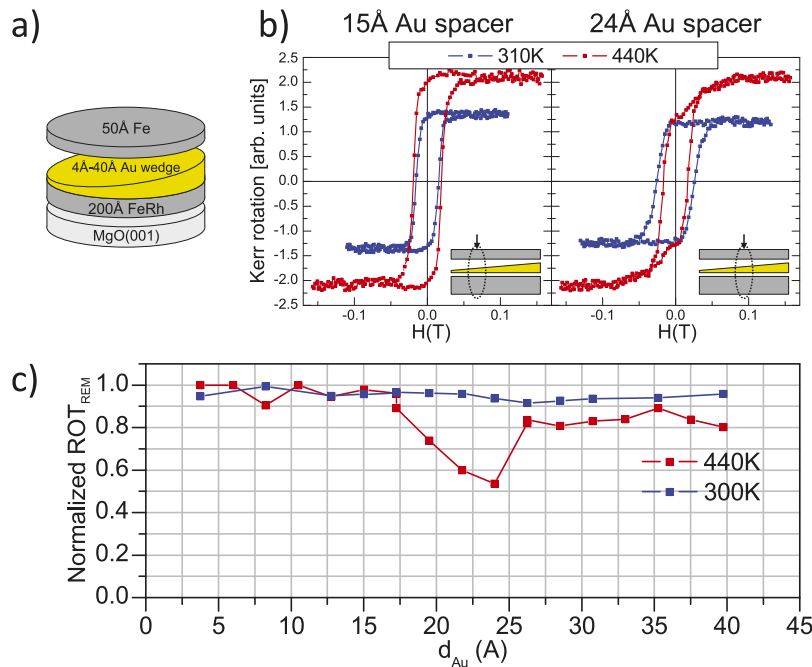


FIG. 2. a) Layered structure of the sample. b) The magnetic hysteresis loops collected for the selected Au spacer thicknesses, $d_{\text{Au}} = 15 \text{ \AA}$ and 24 \AA , at temperatures corresponding to the FeRh_{AFM} state (310-K) and FeRh_{FM} state (440-K). c) The dependence of normalized Kerr rotation at the remanence on the spacer thickness d_{Au} for Fe/Au/FeRh.

saturation field and a lower Kerr rotation at the remanence (denoted further as ROT_{REM}), suggests a non-collinear alignment of the FeRh and the Fe magnetization. Such interpretation is supported by the identical shape of the hysteresis loop measured with the magnetic field applied along [010] (not shown). Moreover, the value of remanence Kerr rotation of the discussed loop (red loop acquired for the 24-Å Au) well matches the magnitude of Kerr rotation at saturation measured for $\text{Fe}/\text{Au}/\text{FeRh}_{\text{AFM}}$ (blue loops in Fig. 2b).

This indicates that when the FeRh sublayer undergoes transition from AFM to FM state its magnetization orients orthogonally to the Fe magnetization. This is manifested in the hysteresis loops shape by an increase of the saturation Kerr rotation, while the remanence Kerr rotation remains unchanged with respect to the rectangular hysteresis loops of $\text{Fe}/\text{Au}/\text{FeRh}_{\text{AFM}}$ system. The dependences of the remanence Kerr rotation ROT_{REM} on Au spacer thickness derived from the normalized LMOKE loops are shown in the Fig. 2c for $\text{Fe}/\text{Au}/\text{FeRh}_{\text{AFM}}$ (300-K) and $\text{Fe}/\text{Au}/\text{FeRh}_{\text{AFM}}$ (440-K). The values of normalized ROT_{REM} close to unity derived at 300-K indicate that the Fe film has an easy magnetization direction parallel to $\text{MgO}[100]$ in the whole thickness range of the Au spacer. Taking into account that the Fe lattice is rotated by 45° with respect to the MgO lattice, the [100] direction of MgO is parallel to the [110] in-plane direction of Fe. This indicates that the [110] direction of the Fe is the easy magnetization direction, in contrast to Fe/MgO systems, where it is known that the easy magnetization axis within the (001) plane is along the [100] Fe direction.¹³ The effect of rotation of the Fe easy magnetization axis can be interpreted as arising from a magnetic interaction with the AFM spin structure of FeRh. Such a spin-flop coupling that was previously reported for Fe/FeRh films is here mediated by the Au spacer.¹⁴ Our interpretation assumes that the in-plane magnetic anisotropy of the FeRh favours the [010] spin orientation. At temperature above the AFM-FM transition temperature (440-K), the ROT_{REM} vs d_{Au} dependence is more complex and lowered values of normalized ROT_{REM} are clearly seen in the vicinity of $d_{\text{Au}} = 24 \text{ \AA}$. The maximum angle between magnetization of the Fe and FeRh films can be roughly estimated to 90° . The ROT_{REM} vs d_{Au} dependence is clearly non-monotonous indicating oscillatory interlayer coupling between Fe and FeRh magnetizations. It is difficult to judge on the origin of non-collinear magnetic coupling (instead of collinear-antiferromagnetic one) but one of possible interpretations assumes that this is a

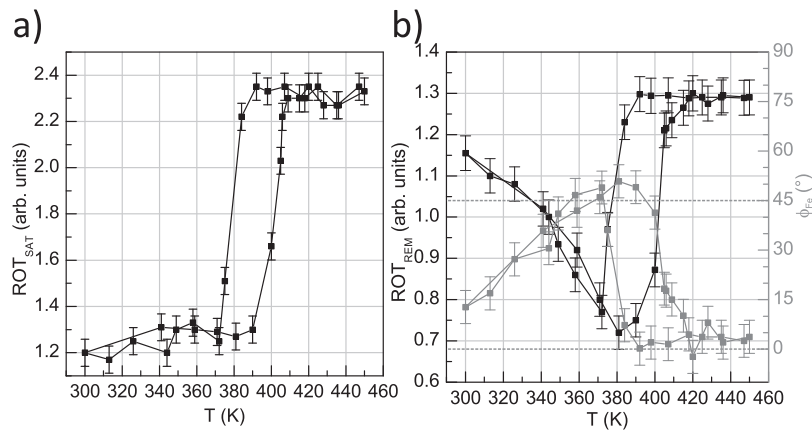


FIG. 3. a) The temperature dependence of ROT_{SAT} for Fe/Au (24-Å)/FeRh. b) The temperature profile of ROT_{REM} for Fe/Au (24-Å)/FeRh. The grey curve and scale on the right indicate the temperature dependence of the angle between Fe magnetization and [100] direction.

roughness induced effect.¹⁵ Finally, the evolution of magnetic structure of the Fe/Au/FeRh system for the Au spacer thickness $d_{Au}=24\text{-}\text{\AA}$ (corresponding to the maximum angle between Fe and FeRh magnetizations manifested in the Fig. 2c by the minimum of normalized ROT_{REM}) was investigated via collection of hysteresis curves during the temperature cycle 300-K – 450-K – 300-K. The temperature dependences of ROT_{SAT} and ROT_{REM}, determined from the measured LMOKE loops, are shown in Figs. 3a and 3b, respectively. ROT_{SAT}(T) reflects the AFM-FM phase transition in the Fe/Au/FeRh system with a similar temperature profile to the Au/FeRh system (compare Fig. 1b). Assuming orthogonal orientation of the Fe and FeRh magnetizations across the AFM-FM phase transition, the shape of the ROT_{REM}(T) curve delivers information about the top Fe magnetization direction. From the ratio of ROT_{REM}(T) to the magnitude of the Fe Kerr rotation signal estimated from low temperature part of ROT_{SAT}(T) dependence (corresponding to the AFM state of FeRh) the temperature driven profile of the angle φ_{Fe} between Fe magnetization and [100] direction can be determined as shown in Fig. 3b with grey.

Following the $\varphi_{Fe}(T)$ dependence a double in-plane reorientation of the Fe magnetization can be seen. First, with increasing temperature the Fe magnetization rotates from [100] at 300K to almost [110] at 380K. We interpret this process as arising from the weakening of the spin flop coupling (that stabilizes the [100] magnetization direction at 300K) as temperature approaches the AFM-FM transition temperature. The magnetization state just below the AFM-FM transition (at 380K for heating branch) corresponds to the intrinsic easy direction of Fe within the (001) plane. The second reorientation of the Fe magnetization, backward towards [100], is clearly a combined effect of appearing ferromagnetism in FeRh at the AFM-FM phase transition and orthogonal magnetic coupling mediated by the Au spacer. Following the cooling branch of the $\varphi_{Fe}(T)$ dependence, the inverse reorientation sequence can be observed. It is clear that Fe reorientation is induced by the AFM-FM phase transition being characterized by a thermal hysteresis, giving a chance to control the Fe magnetization direction with temperature in a similar way as in Ref. 10. For example, at 390K, the Fe magnetization direction along [100] or [110] can be stabilized on cooling and heating branches, respectively.

In conclusion we show that the performance of spin valves structures can be strongly enriched by implementation of the FeRh sublayers. In such spin valves the sublayer magnetization direction can be steered by the AFM-FM phase transition in the FeRh film.

This work is supported by the National Science Center Poland under Project No. 2015/19/B/ST3/00543 and partially by the AGH University of Science and Technology statutory task No. 11.11.220.01/6 within subsidy of the Ministry of Science and Higher Education.

¹ J. S. Kouvel and C. C. Hartelius, *J. Appl. Phys.* **33**, 1343 (1962).

² M. Fallot, *Ann. Phys.* **10**, 291 (1938).

³ M. Fallot and R. Hocart, *Rev. Sci.* **77**, 498 (1939).

- ⁴ A. I. Zakharov, A. M. Kadomtseva, R. Z. Levitin, and E. G. Ponyatovskii, *Sov. Phys. JETP* **19**, 1348 (1964).
- ⁵ M. R. Ibarra and P. A. Algarabel, *Phys. Rev. B* **50**, 4196 (1994).
- ⁶ J. S. Kouvel, *J. Appl. Phys.* **37**, 1257 (1966).
- ⁷ M. P. Annaorazov, S. A. Nikitin, A. L. Tyurin, K. A. Asatryan, and A. K. Dovletov, *J. Appl. Phys.* **79**, 1689 (1996).
- ⁸ J. Thiele, S. Maat, and E. E. Fullerton, *Appl. Phys. Lett.* **82**, 2859 (2003).
- ⁹ M. H. Kryder, E. C. Gage, T. W. Mcdaniel, W. A. Challener, R. E. Rottmayer, G. Ju, Y. T. Hsia, and M. F. Erden, *Proc. IEEE* **96**, 1810 (2008).
- ¹⁰ P. Drózdź, M. Ślęzak, K. Matlak, B. Matlak, K. Freindl, D. Wilgocka-Ślęzak, N. Spiridis, J. Korecki, and T. Ślęzak, *Phys. Rev. Appl.* **9**, 034030 (2018).
- ¹¹ M. Loving, M. A. De Vries, F. Jimenez-Villacorta, C. Le Graët, X. Liu, R. Fan, S. Langridge, D. Heiman, C. H. Marrows, and L. H. Lewis, *J. Appl. Phys.* **112**, 043512 (2012).
- ¹² F. Pressacco, V. Uhlř, M. Gatti, A. Bendounan, E. E. Fullerton, and F. Sirotti, *Sci. Rep.* **6**, 22383 (2016).
- ¹³ J. L. Costa-Krämer, J. L. Menéndez, A. Cebollada, F. Briones, D. García, and A. Hernando, *J. Magn. Magn. Mater.* **210**, 341 (2000).
- ¹⁴ V. Kuncser, W. Keune, B. Sahoo, E. Duman, M. Acet, F. Radu, M. Valeanu, O. Crisan, and G. Filoti, *J. Magn. Magn. Mater.* **272-276**, 348 (2004).
- ¹⁵ S. O. Demokritov, *J. Phys. D: Appl. Phys.* **31**, 925 (1998).